Articles

The EPR Spectrum of Tyrosine Z$^{\bullet}$ and Its Decay Kinetics in O_2-Evolving Photosystem II Preparations[†]

Nikolaos Ioannidis, Georgia Zahariou, and Vasili Petrouleas*

Institute of Materials Science, NCSR "Demokritos", 153 10 Aghia Paraskevi Attikis, Greece

Received March 6, 2008; Revised Manuscript Received April 16, 2008

ABSTRACT: The O_2-evolving complex of photosystem II, Mn_4Ca, cycles through five oxidation states, S_0,..., S_4, during its catalytic function, which involves the gradual abstraction of four electrons and four protons from two bound water molecules. The direct oxidant of the complex is the tyrosine neutral radical, $Y_Z^{\bullet}$, which is transiently produced by the highly oxidizing power of the photoexcited chlorophyll species P_{680}. EPR characterization of $Y_Z^{\bullet}$ has been limited, until recently, to inhibited (non-oxygen-evolving) preparations. A number of relatively recent papers have demonstrated the trapping of $Y_Z^{\bullet}$ in O_2-evolving preparations at liquid helium temperatures as an intermediate of the S_0 to S_1, S_1 to S_2, and S_2 to S_3 transitions. The respective EPR spectra are broadened and split at $g \sim 2$ by the magnetic interaction with the Mn cluster, but this interaction collapses at temperatures higher than about 100 K [Zahariou et al. (2007) *Biochemistry 46*, 14335−14341]. We have conducted a study of the Tyr Z$^{\bullet}$ transient in the temperature range 77−240 K by employing rapid or slow EPR scans. The results reveal for the first time high-resolution X-band spectra of Tyr Z$^{\bullet}$ in the functional system and at temperatures close to the onset of the S-state transitions. We have simulated the $S_2Y_Z^{\bullet}$ spectrum using the simulation algorithm of Svistunenko and Cooper [(2004) *Biophys. J. 87*, 582−595]. The small $g_x = 2.00689$ value inferred from the analysis suggests either a H-bonding of Tyr Z$^{\bullet}$ (presumably with His190) that is stronger than what has been assumed from studies of Tyr D$^{\bullet}$ or Tyr Z$^{\bullet}$ in Mn-depleted preparations or a more electropositive environment around Tyr Z$^{\bullet}$. The study has also yielded for the first time direct information on the temperature variation of the $Y_Z^{\bullet}/Q_A^-$ recombination reaction in the various S states. The reaction follows biphasic kinetics with the slow phase dominating at low temperatures and the fast phase dominating at high temperatures. It is tentatively proposed that the slow phase represents the action of the $Y_Z^{\bullet}/Y_Z^-$ redox couple while the fast phase represents that of the $Y_Z^{\bullet}/Y_ZH$ couple; it is inferred that Tyr Z at elevated temperatures is protonated at rest. It is also proposed that $Y_Z^{\bullet}/Y_ZH$ is the couple that oxidizes the Mn cluster during the S_1-S_2 and S_2-S_3 transitions. A simple mechanism ensuring a rapid (concerted) protonation of Tyr Z upon oxidation of the Mn cluster is discussed, and also, a structure-based molecular model suggesting the participation of His190 into two hydrogen bonds is proposed.

Photosystem II (PSII) catalyzes a fundamental reaction, the splitting of water which results in the evolution of molecular oxygen. The site of water oxidation, called the oxygen-evolving complex (OEC), contains a tetranuclear Mn cluster and a Ca^{2+} ion. The catalytic cycle of the OEC involves four light-driven one-electron oxidation steps, S_0-S_1,..., $S_3-(S_4)S_0$, accompanied by the progressive removal of four protons from two bound water molecules. The sequence of events for each photochemical step includes the photooxidation of a special chlorophyll species called P_{680}[1] and the transfer of the electron to a series of electron acceptors, namely, pheo (pheophytin), Q_A, and Q_B (primary and secondary plastoquinone electron acceptors). P_{680}^+ in parallel oxidizes rapidly Tyr Z in a time scale of nanoseconds to microseconds; the thus formed Tyr Z$^{\bullet}$ radical regains its electron by oxidizing the Mn cluster in a few tens of microseconds for the S_0 to S_1 transition, to ~1 ms for the S_3 to $(S_4)S_0$ transition. Oxygen evolves during the latter transition, with the S_4 being a transient state (*1*–*5*). A critical limiting factor in the water-splitting reactions is the requirement of efficient removal of the protons from the substrate water along with the four one-electron oxidation steps (see, e.g., refs *5* and *6* for a summary).

[†] Financial support of the programs AKMWN and BRD of the Greek GSRT is kindly acknowledged.

* Corresponding author. Tel: +301 650-3344. Fax: +301 651-9430. E-mail: vpetr@ims.demokritos.gr.

[1] Abbreviations: Tyr Z or Y_Z, tyrosine 161 of the D2 protein; Tyr D or Y_D, tyrosine 160 of the D1 protein; P_{680}, the primary electron donor in PSII; signal II, the EPR signal of Tyr D$^{\bullet}$ at X-band frequencies; pheo, pheophytin primary electron acceptor; Q_A and Q_B, the primary and secondary plastoquinone electron acceptors of PSII; chl^+ and car^+, chlorophyl and carotenoid cation radicals; MES, 2-*N*-morpholineethanesulfonic acid; duroquinone, tetramethyl-*p*-benzoquinone; EPR, electron paramagnetic resonance.

10.1021/bi800390r CCC: $40.75
Published on Web 05/22/2008

Tyr Z has been at the focus of considerable interest in recent years. It lies in close proximity to Mn, and also its redox function is coupled to (de)protonation reactions (*7*), as suggested by the considerable difference between its pK_{ox} (−2) and pK_{red} (∼10). Suggestions about the proton-coupled redox function of Tyr Z have varied. The simplest assumption is that the phenolic proton moves back and forth between Tyr Z and a nearby base, D1 His190, during oxidation and reduction of Tyr Z. This rocking proton hypothesis, originally suggested by Eckert and Renger (*8*), was largely based on time-resolved optical spectroscopy and proton release measurements (*9, 10*). An advanced hypothesis has assumed an active role for Tyr Z in the water-splitting reactions (*11, 12*). According to the model advanced by the late G. Babcock and colleagues, a hydrogen atom (i.e., a proton plus an electron) is abstracted from the OEC by Tyr Z• at each S-state transition (*11*). The acquired electron is transferred to P_{680}^+, while the proton is transferred to His190 and from there to the lumen via a series of consecutive charged amino acid residues. Recent findings including crystallographic and spectroscopic results have questioned the validity of the hydrogen atom abstraction model at least for the lower S state transitions (*13, 14*). The rocking motion appears, accordingly, to be the most plausible hypothesis with an important addition, however. A number of considerations, based on phenomenology (*14*) and on thermodynamic grounds (*5*), suggest the coupling of the e^-/H^+ transfer reactions at the Mn and Tyr Z sites. During a typical S-state transition an electron is transferred from Mn to Tyr Z•, a proton presumably from His190 neutralizes Tyr Z^-, and another proton is removed from the Mn cluster. There will be a clear thermodynamic advantage if the one-electron two-proton transfer reactions occur in a concerted way. Not only is the operating potential of the redox couple $Y_Z^•/Y_ZH$ much higher than that of the couple $Y_Z^•/Y_Z^-$ but also the synchronization of the electron/proton transfer reactions at the Mn site eliminates high-energy intermediates (*5*). A serious limitation so far in evaluating the role of Tyr Z in the water-splitting reactions has been the difficulty of probing it spectroscopically in the intact system due to the short lifetime of the Tyr Z• radical at ambient temperatures. Hoganson and Babcock (*15*) recorded EPR spectra of this tyrosine at room temperature by employing gated integration techniques. The spectra obtained from intact preparations were too noisy to extract useful information except to say that they were not too different from the spectrum of Tyr D•.

Rather extensive studies have been conducted on Tyr Z• in inhibited preparations. In these preparations Tyr Z• can be trapped by brief illumination at temperatures close to 0 °C and subsequent cooling and is indefinitely stable at cryogenic temperatures. High-resolution spectra have been reported and characterized in Mn-depleted Y_D-less *Synechocystis* samples (*16, 17*) and in Mn-depleted samples from *Chlamydomonas reinhardtii* (*18*) and *Thermosynechococcus elongatus* (*19*). Clear differences between Tyr Z• and Tyr D• are observed at X-band EPR frequencies, where the spectra are dominated by the hyperfine interactions, and also at high-frequency EPR, where the resolution among the *g*-value components is enhanced (*19, 20*). A direct conclusion from these studies is that both radicals are hydrogen bonded; a broadening in the g_x value of Tyr Z• has been attributed to a disorder in the local protein environment. The situation is less clear in samples inhibited by the more mild treatments of Ca^{2+} removal or acetate treatment. The spectra of Tyr Z• at liquid helium temperatures are dominated by magnetic splitting, due to the magnetic interaction with the Mn cluster (refs *21–25* and *26*, where an alternative origin of the magnetic interaction is assumed). At elevated temperatures, the magnetic interaction with Mn averages out due to the fast relaxation of the Mn spin (*27*), and X-band EPR spectra similar to that of Tyr D• have been reported (*28–30*). The possibility, however, of severe interference from Tyr D•, which is also oxidized under the illumination conditions that are employed to oxidize Tyr Z in this case, has been raised (*19*). Simulations of the magnetically split spectra at high-frequency EPR, on the other hand, suggest heterogeneity in the g_x values of Tyr Z• (*19*). In all of the above cases the Tyr D• parameters appear to be unaltered compared to intact preparations. Because of the uncertainties in the line shape of Tyr Z• in the available EPR spectra from inhibited preparations, and the importance of this radical in the water-splitting reactions, it has been highly desirable to obtain spectra of Tyr Z• in oxygen-evolving preparations.

Recent advances have provided a wealth of Tyr Z• EPR signals in intact preparations, all at liquid helium temperatures (*31–47*). The spectra show magnetic splittings with distinct features for each S state. The analysis of the magnetic interaction has yielded so far interesting information about the magnetic coupling with the Mn cluster (*39, 41*), and the phenomenology of the Tyr Z• trapping has provided important clues on thermal constraints associated with Tyr Z oxidation (*14, 42*). However, the spectra cannot be used easily to obtain information on the electronic configuration of Tyr Z as the fine and hyperfine features of the $Y_Z^•$ spectrum are obscured by the magnetic interaction with the Mn cluster. In a recent study (*47*) we showed that all of the $S_nY_Z^•$ ($n = 0, 1, 2$) signals narrow with increasing temperature above liquid helium temperatures, and at about 100−120 K the spectra collapse to a 25 G radical spectrum attributed to the magnetically isolated Tyr Z• radical. This is due to the averaging of the magnetic interaction with the Mn cluster due to the increase of the spin−lattice relaxation rate of the spin of the Mn cluster with increasing temperature (see also refs *27* and *48*).

We have undertaken a study aimed at trapping and resolving the spectrum of Tyr Z• at elevated temperatures in all S states that exhibit a split signal at liquid helium temperatures. A combination of slow and rapid scan EPR has been applied to record the transient spectra at temperatures as high as 240 K. This study has also yielded for the first time direct information on the temperature variation of the $Y_Z^•/Q_A^-$ recombination reaction in the various S states. Implications of the results on the H-bonding environment of Tyr Z and the forward reactions are discussed.

MATERIALS AND METHODS

PSII Sample Isolation. PSII-enriched thylakoid membranes were isolated from spinach (see ref *49*, with modifications). Samples for EPR measurements were suspended in 0.4 M sucrose, 15 mM NaCl, 5 mM $MgCl_2$, and 40 mM MES, pH 6.5, at about 6−8 mg of chl/mL and stored in liquid nitrogen. All samples were supplemented with 1 mM duroquinone (dissolved in DMSO) as an exogenous electron acceptor.

Sample Treatments. Methanol (5% v/v) was added when specifically indicated. Glycerol-treated samples were resuspended and washed twice in a buffer containing 50% glycerol, 15 mM NaCl, 5 mM $MgCl_2$, and 40 mM MES, pH 6.5, at 6−8 mg of chl/mL. The NO treatment was carried out to samples that were advanced to the S_0 state after the administration of the three flashes. NO was added in order to reduce the contaminating S_2 and S_3 states to the S_1 state (*50*). The addition was done anaerobically at 0 °C inside the EPR tubes by slowly bubbling 4 mL of a 1:5 mixture of NO and N_2 for 1−2 min.

Illumination Conditions. Two studio photographic power supplies were used for flash excitation of samples: a 600 W with pulse duration of 2.1 ms, at temperatures below ca. 220 K, and a 200 W with pulse duration of 1.2 ms, at temperatures above 220 K. The latter produced single turnovers at −5 °C. For continuous illumination a 360 W projection lamp filtered with a saturated solution of $CuSO_4$ was used.

The S_2Q_A (±MeOH) state was produced by single-flash illumination at −5 °C of the S_1 state, followed by 30 s incubation at the same temperature, in the dark, to allow electron transfer from Q_A^- to duroquinone. This produced ∼80% of S_2 and no detectable amounts of S_3 (as judged by the EPR spectrum recorded at 10 K). S_2 was subsequently maximized by a strong flash at 190 K followed by 1 min dark adaptation at the same temperature before transfer to −5 °C for 30 s. The S_0Q_A (+MeOH) state was produced by administration of three flashes, spaced by 30 s, to the S_1 state at −5 °C.

All Tyr Z$^\bullet$-based intermediates were produced by direct illumination of the respective S state at the temperature examined. In earlier studies the $S_2Y_Z^\bullet$ intermediate was produced by flash illumination at temperatures higher than 77 K and immediate transfer to liquid nitrogen and from there into the EPR cryostat at 10 K (*42, 47*). This procedure was not necessary here because all experiments were performed above 77 K.

Elimination of Contributions from Other Radical Species. Illumination at cryogenic temperatures produces, in addition to the Tyr Z$^\bullet$ radical, small amounts of the chl^+ and car^+ cation radicals. These are less efficient electron donors, and the use of flash excitation minimizes their production (*35*). The EPR signals of these species are narrow and can be easily discerned when present. These signals saturate easily and decay more slowly than the Tyr Z$^\bullet$ radical signal under examination. Contribution of these minority species was eliminated by the use of high microwave power and difference spectroscopy. Cyt b_{559} is also oxidized to a small extent, but its spectrum has no spectral overlap with the S_nY_Z radicals. To minimize accumulation of the charge-separated state Cyt $b_{559}^+...Q_A^-$ during the recording of the $S_2Y_Z^\bullet$ intermediate under continuous illumination, Cyt b_{559} was preoxidized by prolonged intense illumination at 77 K followed by 30 s dark adaptation at −5 °C to allow for oxidation of Q_A^- by the exogenous quinone.

EPR Measurements. EPR measurements were obtained with an upgraded Bruker ER-200D spectrometer interfaced to a personal computer and equipped with an Oxford ESR 900 cryostat (either liquid helium or liquid nitrogen was used for temperature control), an Anritsu MF76A frequency counter, and a Bruker 035M NMR gaussmeter. The signal-channel unit was replaced with an SR830 digital lock-in amplifier by Stanford Research. The perpendicular 4102ST cavity was used, and the microwave frequency was 9.41 GHz. In the rapid scan experiments the data were recorded by a multifunction NI 6251 pci card by National Instruments (16 bit/1.25 MS/s) mounted on a personal computer running appropriate software in the LabView programming environment. Synchronization of the data acquisition with the magnetic field ramp produced by the time base unit was achieved by triggering the AD converter with a TTL pulse produced by the time base unit at the beginning of each scan. The minimum duration possible for each scan was 20 ms with a delay of 20 ms between the scans.

In rapid scan mode, variable temperature spectra were collected prior to and after flash illumination. The spectra of the $S_nY_Z^\bullet$ intermediates were constructed by averaging 10 spectra obtained immediately after the flash (omitting the first one) and subtracting the average of several spectra obtained when the intermediate had decayed.

In slow scan mode, spectra were obtained under illumination and after illumination. The spectra of the $S_nY_Z^\bullet$ intermediates were obtained by suitable light minus dark subtractions (see Figure S1 in Supporting Information for an example). Spectral noise was reduced by addition of several runs.

Simulation. Spectra of Tyr Z$^\bullet$ and Tyr D$^\bullet$ (as control) were simulated using the program simpow6 (Mark Nilges, Illinois EPR Research Center, http//:ierc.scs.uiuc.edu/∼nilges/software.html). The results obtained from these simulations were refined by the use of the algorithm of Svistunenko and Cooper (*51*), according to which the tyrosyl radical spectrum can be simulated by searching for suitable values for the spin density ρ on atom C1 and the phenoxyl ring rotation angle θ. The values of ρ and θ are subsequently used for the estimation of the principal values of the g vector and the hyperfine interaction values of the two β-methylene protons.

RESULTS

The Spectrum of the Tyr Z$^\bullet$ Radical at Elevated Temperatures. In a recent study (*47*) we showed that the Tyr Z$^\bullet$-based transient signals in intact preparations collapse at about 100−120 K to a radical spectrum, with a 25 G width, which is attributed to the magnetically isolated Tyr Z$^\bullet$ radical. Low-resolution spectra of the magnetically isolated tyrosyl radical were presented for the $S_2Y_Z^\bullet$ intermediate at 140 and 190 K. We have examined closely the spectra of the various Tyr Z$^\bullet$ intermediates, including those modified by the presence of methanol, at elevated temperatures. Low modulation amplitude was employed in order to enhance the resolution of the spectra. Representative spectra obtained in rapid scanning mode, at 130−140 K, with a modulation amplitude of 4 Gpp are shown in Figure 1; the spectrum of the unsaturated Tyr D$^\bullet$ is included for comparison. The spectra appear similar within experimental uncertainty (the small differences present will be evaluated in future studies). The spectra are reminiscent of those obtained in Mn-depleted samples (*17–20*), in which Tyr Z$^\bullet$ can only be induced by high-temperature illumination and trapped by rapid freezing. Rather surprisingly, they differ from those of Tyr Z$^\bullet$ in preparations inhibited by more mild treatments, such as

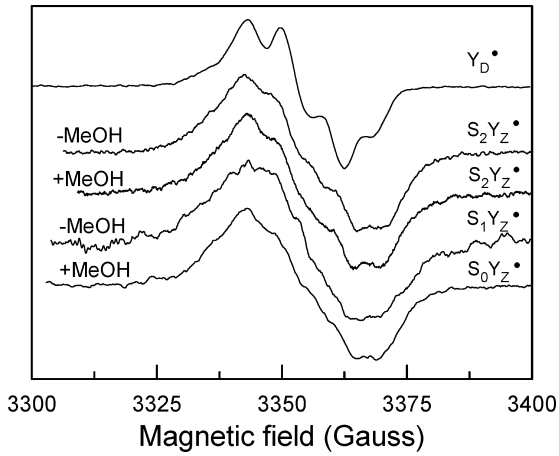

FIGURE 1: Tyr Z• light minus dark difference spectra at 130−140 K in various S states compared with the spectrum of Tyr D•. Rapid scanning EPR conditions: modulation amplitude, 4 Gpp; microwave power, 100 mW ($Y_Z^•$) or 0.013 mW ($Y_D^•$); microwave frequency, 9.41 GHz; modulation frequency, 100 kHz; sweep field width, 100 G; sweep time, 200 ms; time constant, 1 ms.

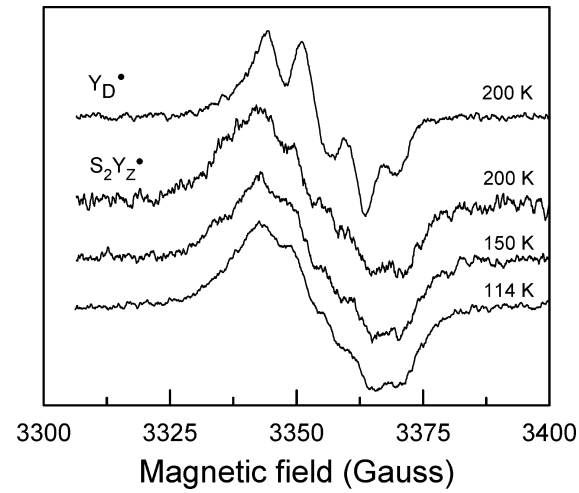

FIGURE 2: High-resolution light minus dark difference EPR spectra of $S_2Y_Z^•$ at three different temperatures compared with signal II (the spectrum of Tyr D• recorded under nonsaturating conditions). The $S_2Y_Z^•$ spectra show distinct features that are reproduced at all temperatures. EPR conditions: modulation amplitude, 2 Gpp; microwave power, 100 mW for the $Y_Z^•$ spectra and 0.013 mW for the $Y_D^•$ spectrum; microwave frequency, 9.41 GHz; modulation frequency 100 kHz; sweep field width, 100 G; sweep time, 50 s; time constant, 300 ms.

acetate (*27*) and formate (*29*) addition or calcium depletion (*30*). The latter spectra appear to be similar to those of Tyr D•, although the difficulty in removing contributions from Tyr D• which is inevitably oxidized during the high-temperature illumination/rapid-freeze protocols used to trap Tyr Z• in all the inhibited preparations has been noted (*19*).

The $S_2Y_Z^•$ radical can also be observed in samples containing 50% (v/v) glycerol (spectra not included). No significant deviations are observed from the properties of the respective intermediate in untreated samples except for a somewhat broader splitting at 11 K (126 G wide in the presence of glycerol compared with 116 G for the untreated sample).

To enhance further spectral resolution, we also used lower modulation amplitude. The decreased signal-to-noise ratio was overcome by the use of slow scans and collection of the spectra under steady-state conditions, i.e., during continuous illumination (see the Materials and Methods section). Figure 2 shows the spectra of Tyr Z• at three different temperatures, recorded with a 2 Gpp modulation amplitude. The unsaturated spectrum of Tyr D• is included for comparison. The features of the Tyr Z• spectrum remain practically unchanged in the range 114−200 K, confirming the earlier observation that the magnetic interaction with the Mn cluster averages out completely above about 120 K.

Analysis of the Spectra. A large set of parameters is needed to simulate a tyrosyl EPR spectrum. The line shape of the spectrum depends on the principal values of the g vector and the hyperfine interaction of the unpaired electron with the four phenoxyl ring protons and the two β-methylene protons. The hyperfine interaction with the β-methylene protons is modulated by the rotation angle θ and the spin density ρ on carbon atom C1 (Scheme 1). Svistunenko and Cooper (*51*) have developed empirical relationships between the whole set of parameters of the tyrosyl spectrum and the two independent parameters, ρ_{C1} and θ. Most importantly, they have noted a linear relationship between ρ_{C1} and g_x.

We have chosen to simulate two spectra: Tyr D• (signal II) and $S_2Y_Z^•$. We first did extensive search over the parameter space using the program simpow6 and later applied the Svistunenko and Cooper approach by searching for

Scheme 1: Phenoxyl Ring Rotation Angle θ in Tyrosine

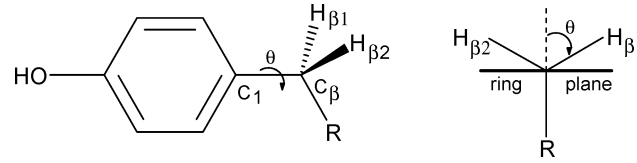

different values of ρ_{C1} and θ and generating spectra that were compared to the experimental ones. Both approaches converged to approximately the same best parameter set. The results are depicted in Figure 3. The simulation for both radicals is clearly very satisfactory. The parameter values resulting from the simulation are evaluated in the Discussion section.

Decay Kinetics of Tyr Z•. Rapid scans offer a reliable method to study the decay kinetics of a signal devoid of baseline drifts (a common problem in EPR spectroscopy), since they record full spectra at each time point. Figure 4 shows the spectrum of the $S_2Y_Z^•$ transient formed by flash illumination of the S_2 state at 200 K (red trace), superimposed on the background signal of Tyr D• (black trace), appropriately scaled down. The spectra are recorded at high microwave power (100 mW) and relatively high modulation amplitude, 8 Gpp, to enhance the signal-to-noise ratio. Under these conditions the Tyr D• signal is saturated, while that of Tyr Z• is not, as will be discussed later. The inset of Figure 4 depicts the decay kinetics of the Tyr Z• signal at 190 K, pooled from six experiments. The difference in intensity at field values 3340 and 3300 G (arrows in Figure 4) was taken as a measure of the Tyr Z• signal intensity (other suitable differences exhibited similar behavior). A double exponential curve (solid line) is fitted to the data with half-times of 0.8 s (73%) and 9.5 s (27%).

We have studied the decay kinetics of Tyr Z• in the various S states at representative temperatures in the range 70−240 K in a manner similar to that depicted in Figure 4. The data are summarized in Table 1. It is noted that the decay rate is

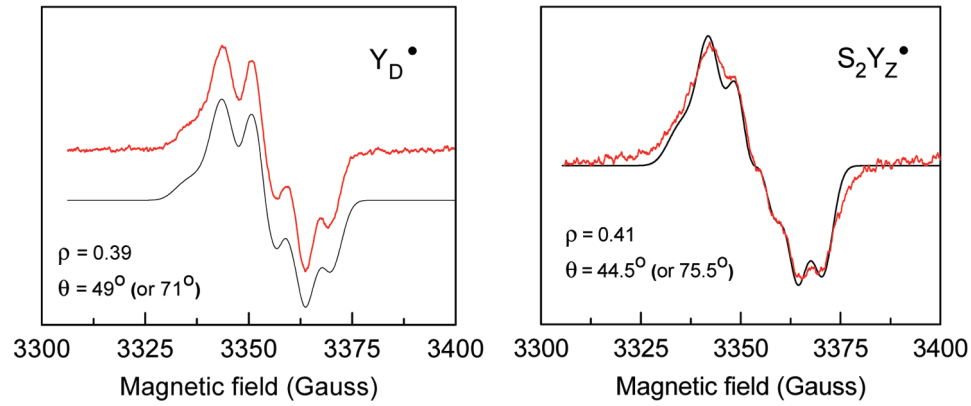

FIGURE 3: Experimental (red) and simulated (black) spectra of the $Y_D^\bullet$ and the $S_2Y_Z^\bullet$ tyrosyl radicals. EPR conditions: modulation amplitude, 2 Gpp; microwave power, 100 mW for the $Y_Z^\bullet$ spectrum and 0.00317 mW for the $Y_D^\bullet$ spectrum; microwave frequency, 9.41 GHz; modulation frequency, 100 kHz; sweep field width, 100 G; sweep time, 50 s; time constant, 300 ms; temperature, 150 K for $Y_D^\bullet$ and 114 K for $Y_Z^\bullet$. Simulation parameters for the $Y_D^\bullet$ spectrum: $g_x = 2.00763$, $g_y = 2.00431$, $g_z = 2.00231$, $A_{||}^{\beta 1} = 29.76$ MHz, $A_{\perp}^{\beta 1} = 26.40$ MHz, $A_{||}^{\beta 2} = 10.57$ MHz, $A_{\perp}^{\beta 2} = 4.45$ MHz. Simulation parameters for the $Y_Z^\bullet$ spectrum: $g_x = 2.00689$, $g_y = 2.00418$, $g_z = 2.00221$, $A_{||}^{\beta 1} = 36.63$ MHz, $A_{\perp}^{\beta 1} = 32.37$ MHz, $A_{||}^{\beta 2} = 7.51$ MHz, $A_{\perp}^{\beta 2} = 2.49$ MHz.

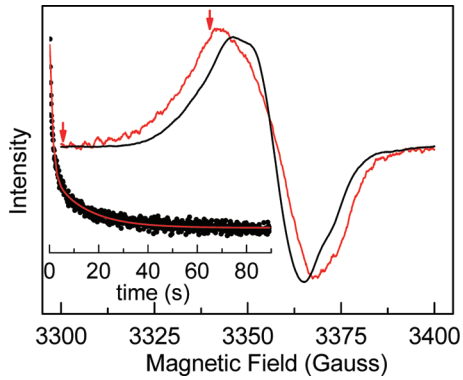

FIGURE 4: Transient signal, $S_2Y_Z^\bullet$, formed by flash illumination of the S_2 state at 190 K (red trace), compared with the background signal (signal II). The latter signal has been scaled down to match the $S_2Y_Z^\bullet$ signal intensity. Inset: Decay kinetics of the $S_2Y_Z^\bullet$ EPR signal at the same temperature. Data points represent the intensity difference at 3340 and 3300 G (average of six runs). The flash was given at time 0. A double exponential curve (solid line) is fitted to the data with half-times of 0.8 s (73%) and 9.5 s (27%). Rapid mode EPR conditions: modulation amplitude, 8 Gpp; microwave power, 100 mW; microwave frequency, 9.41 GHz; modulation frequency, 100 kHz; sweep field width, 100 G; sweep time, 100 ms; time constant, 0.3 ms.

biphasic in all cases, but the relative amplitude of the two phases varies with temperature. The amplitude of the fast phase is small at 70 K but increases with increasing temperature and dominates at about 200 K. Extrapolation to higher temperatures suggests that at temperatures above 0 °C only the fast component will be present. In addition to the change in the relative amplitude of the two phases, the signal decay $t_{1/2}$ decreases considerably with increasing temperature.

$S_1Y_Z^\bullet$ is an exception to the general behavior of the intermediates in Table 1. This is because the S_1 to S_2 state transition becomes activated above about 77 K; therefore, the percentage of the radical, which can be trapped under these experimental conditions, is diminished with increasing temperature, as was mentioned in our earlier study (*47*).

It should be noted that the absolute $t_{1/2}$ values vary somewhat among different preparations. The relative trends [temperature variation of the two phases, faster decay for $S_2Y_Z^\bullet$ (+MeOH)] are, however, entirely reproducible. An extended set of data for the case of $S_2Y_Z^\bullet$ is presented as an Arrhenius plot in Figure S2 in Supporting Information.

Power Saturation Properties of the Tyr Z• Signal. A common feature of all Tyr Z•-based metalloradical signals is that they do not saturate easily at 10 K (*33, 35, 42*). This is due to the enhancement of the relaxation properties of Tyr Z• by the Mn cluster. We have examined the saturation properties of the high-temperature Tyr Z• spectra. No systematic power saturation studies could be made due to uncertainties in the signal intensity at low microwave power. The normalized signal intensity (intensity over square root of power), however, was practically independent of the microwave power in the range 6−100 mW, above about 70 K (see Figure S1 in Supporting Information for spectra of $S_2Y_Z^\bullet$ obtained at 150 K). By comparison, the signal of Tyr D• is strongly saturated. The contrasting behavior of the Tyr Z• is entirely consistent with its proximity to Mn. The elevated temperature averages out the magnetic interaction with the Mn but not the relaxation enhancement (*48*).

DISCUSSION

Tyr Z and H-Bonding. The spectra of the various Tyr Z• radicals reported here are similar within experimental uncertainty (Figure 1). This implies that no major conformational changes occur in Tyr Z• among the various S states. It should be noted, however, that, unlike the partially resolved hyperfine structure, the resolution of the *g* values of a tyrosyl radical is poor at X-band EPR spectroscopy. Clearly, a conclusive evaluation has to await high-field EPR characterization, which may not be easily applicable in the present case.

The spectral characteristics of the radicals are different from those of Tyr Z• in mildly inhibited preparations [acetate- (*22, 27*) or formate-treated (*29*), calcium-depleted (*26, 28, 30*)] but surprisingly resemble those of Tyr Z• in Mn-depleted samples (*17, 19*). The latter have been rather extensively studied with a variety of EPR methods. It would be interesting to compare our preliminary analysis of the $S_2Y_Z^\bullet$ and $Y_D^\bullet$ spectra, based on the empirical methods of Svistunenko and Cooper (*51*) (see Figure 3), with the results reported in the literature for Tyr D• and Tyr Z• in Mn-depleted samples.

Table 1: Variation of the Decay Kinetics of the $S_nY_Z^•$ Radicals with Temperature[a]

	$t_{1/2}$ slow (s), $t_{1/2}$ fast (s)				
T (K)	$S_0Y_Z^•$ (+MeOH)	$S_1Y_Z^•$	$S_2Y_Z^•$	$S_2Y_Z^•$ (+glycerol)	$S_2Y_Z^•$ (+MeOH)
70	48 (82),[a] 7 (18)	120 (81), 9.6 (19)	71 (82), 4.5 (22)		50 (72), 3.2 (28)
90	41 (75), 5.3 (25)	72 (64), 7 (36)		35 (58), 2.5 (42)	36 (55), 1.7 (45)
135	32 (58), 3 (42)	−, 2.7 (100)	55 (60), 3.8 (40)	18 (40), 1.3 (60)	28 (25), 1.3 (75)
190	24 (38), 1.4 (62)		9.5 (27), 0.8 (73)	4.1 (21), 0.3 (79)	
240	7.3 (26), 0.6 (74)		2.5 (20), 0.4 (80)		

[a] Values in parentheses are in percent.

The values of the *g* tensor and the β-methylene hyperfine interactions found for the Tyr D• radical are in reasonable agreement with those reported in the literature (ref *52* and references cited therein). The respective values for the Tyr Z• radical show some notable differences from those reported for Mn-depleted samples (*16, 18*). The rotation angle $\theta = 45.5°$ reported here is quite similar to the one reported in a relatively recent study of Mn-depleted samples (*18*), although an earlier study indicated a rather broad distribution of θ values in the Mn-depleted samples (*16*). It has been suggested that ρ_{C1} values of about 0.38 or greater indicate that the tyrosyl radicals are likely H-bonded, with the strength of the H-bond being greater with higher ρ_{C1} values (*19, 51, 53*). Also, as mentioned in the Results section, a linear relationship has been found between ρ_{C1} and g_x (increased ρ_{C1} values correspond to decreased g_x values) (*51*). Accordingly, both the ρ_{C1} and the $g_x$parameters can be related to the strength of the hydrogen bonding. In the Mn-depleted samples similar ρ_{C1} values of 0.37−0.38 were found for both Tyr D• and Tyr Z• (*16, 18*). A well-structured hydrogen bond was inferred for Tyr D•, whereas in Tyr Z• a distribution of hydrogen-bonding distances and thus strengths was proposed (*16, 17*). This proposal was supported by high-field EPR experiments, which showed a broad g_x edge in Tyr Z• spectra of Mn-depleted samples from spinach, *Synechocystis* PCC 6803, and *T. elongatus* (*19*). In our intact system, a ρ_{C1} value of 0.39 is found for Tyr D•, in reasonable agreement with the literature values, while a value of 0.41 is estimated for the Tyr Z• radical. The latter is larger than the reported values in the Mn-depleted preparations. In accordance with the increased ρ_{C1} value, our estimation of g_x (=2.00689) is smaller than the $g_x = 2.0071$ reported for the *T. elongatus* in Mn-depleted samples (*19*). This suggests that the hydrogen bond in the case of Tyr Z• in the intact system may be stronger. The fact that smaller g_x values are related to stronger H-bonding is supported by the following observation. γ-Irradiation of tyrosine hydrochloride crystals results in $Tyr^{(•)}$-HCl radical formation with a small g_x value of 2.0067 (*54*). Neutron diffraction performed on these crystals shows that each phenoxyl oxygen is 1.6 Å away from the protonated carboxylic acid of a neighboring tyrosine, indicating strong H-bonding to the phenoxyl oxygen (*55*). Another factor that could contribute to the increase of ρ_{C1} would be a more electropositive environment of Tyr Z• in the intact system (*19*).

The above considerations suggest a stronger H-bonding and/or a more electropositive environment of Tyr Z in the intact system. It should be remembered, however, that the present preliminary analysis has been performed on the $S_2Y_Z^•$ intermediate, for which more resolved spectra are available. The spectra of the other intermediates appear similar to the $S_2Y_Z^•$ (see Figure 1), but subtle differences do exist, and these will be evaluated in future studies. It is possible that the increased ρ_{C1} (small g_x) for the $S_2Y_Z^•$ intermediate reflects the fact that the OEC is more positively charged in S_2 (see later in the Discussion section).

Kinetics of Tyr Z• Recombination. A notable property of the Tyr Z• decay pattern is that it becomes biphasic above about 70 K and the relative amplitude of the fast phase increases with increasing temperature. The transition to the fast phase is completed very early (below 135 K) for $S_1Y_Z^•$, but this is attributed to the onset of the S_1 to S_2 transition. This step, i.e., oxidation of the Mn cluster by Tyr Z•, is probably much faster than the recombination rate of Tyr Z• and beyond the resolution of the present experiments (work in progress). For all other intermediates the transition to the fast phase is gradual. At 190 K the fast phase reaches values of 60−80% (Table 1).

The temperature range of the present experiments is below the threshold for S-state advancement (oxidation of the Mn cluster) with the exception of the S_1 to S_2 step, as mentioned above. Tyr Z• in this temperature range decays presumably by oxidation of P_{680} (following the reverse reaction: $P_{680}^+ + Y_Z \leftrightarrow P_{680} + Y_Z^•$). P_{680}^+ decays subsequently very fast either by recombination with Q_A^- or by oxidation of auxiliary donors such as car or chl or Cyt b_{559}. The rate of decay of Tyr Z• will accordingly be determined by the difference in redox potential between the couples $Y_Z^•/Y_Z$ and P_{680}^+/P_{680}. The redox potential of P_{680}^+/P_{680} was recently revised to 1.25 V (*56, 57*), while that of $Y_Z^•/Y_Z$ varies with its protonation state. The redox potential of the couple $Y_Z^•/Y_Z^-$ should be 300 mV lower than the potential of the couple $Y_Z^•/Y_Z(H)$; a widely acceptable value for the latter is 0.97 V (ref *58*, but see also ref *57* where a value of 1.21 V is estimated for the kinetic redox potential which pertains during the first 10 μs after oxidation). Tyr Z• will accordingly exhibit a fast decay in centers where reduction and protonation of Tyr Z• occur in a concerted way and a slow decay in centers where protonation is constrained and occurs on a slower time scale than reduction. It is likely that the observed slow phase is due to centers undergoing sequential electron−proton transfer during the reduction of Tyr Z• while the fast phase characterizes centers where reduction of Tyr Z• is coupled to protonation (proton-coupled electron transfer, PCET). It is possible that the transition from the slow to fast decay kinetics is triggered by the onset of protein mobility observed above 120 K in PSII membrane fragments (*59*).

Examination of the temperature dependence of the two kinetic phases shows that both phases exhibit very small dependence up to about 140 K, while above this temperature both show moderate dependence. Small activation barriers of 11.6 and 12.5 kJ/mol were estimated from

Scheme 2: Schematic Presentation of the S_1 to S_2 Transition Emphasizing the Proton-Coupled Electron Transfer during the Reduction of Tyr Z$^{\bullet}$ by the Mn Cluster[a]

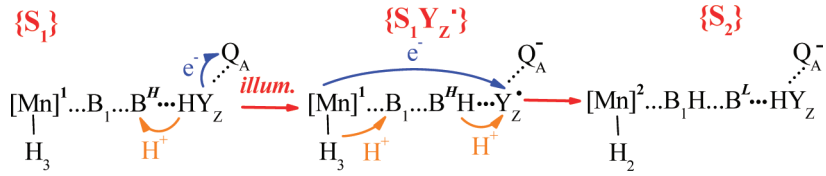

[a] Preservation of the manganese proton in the nearby base B_1 during the S_1 to S_2 transition converts the base partner of Tyr Z (D1 His190) from a high B^H to a low B^L, p*K* form ensuring a concerted reduction/protonation of Tyr Z$^{\bullet}$ and therefore a high operating oxidation potential.

Arrhenius plots (see Figure S2 in Supporting Information) for the fast and slow phase, respectively, which may indicate relaxation processes of a surrounding proton network, in a manner similar to that proposed for the explanation of the "microsecond phase" in the oxidation reaction of Tyr Z by P_{680}^+ (*60*). It is interesting to note that extrapolation of the linear fit of the Arrhenius plot to 21 °C results in $t_{1/2} \approx 97$ ms for the decay of the fast phase. This is close to the value of ~140 ms reported for the recombination between Tyr Z$^{\bullet}$ and Q_A^- in PSII particles from *Synechocystis* sp. (*61*).

The above considerations may answer a long-standing question on whether Tyr Z at rest is protonated or not. It appears that it is protonated, since above about 200 K reduction of Tyr Z$^{\bullet}$ occurs in a concerted way with its protonation, in the majority of centers (see, however, ref *62* for an alternative view).

Implications for the Forward Reactions (S-State Advancement). (A) The S_1 to S_2 Step. The reduction of Tyr Z$^{\bullet}$ by the Mn cluster (above the temperature threshold of the S state transitions) is significantly faster than the recombination reactions studied here (*63*). Therefore, the conclusion about a concerted reduction/protonation of Tyr Z$^{\bullet}$ during recombination cannot be easily extrapolated to the forward reactions. The following considerations can, however, provide useful hints. Two protons move during oxidation of Mn by Tyr Z$^{\bullet}$ during a typical S-state transition, one away from the Mn cluster and the other toward Tyr Z$^-$. Oxidation of the Mn cluster must be coupled to its deprotonation in order to avoid high-energy intermediates (*5*). It is less obvious whether reduction of Tyr Z$^{\bullet}$ is coupled to protonation (reduction and protonation may not be concerted reactions). The advantage of a concerted reaction is the higher oxidizing potential of Tyr Z (see above). The S_0 to S_1 transition may not need the extra oxidizing potential since the E_m of this transition is ~0.7 V (*64*). The S_1 to S_2 and S_2 to S_3 transitions have high oxidation potentials [0.90−0.95 V (*64*)], and exploitation of the full redox potential of Tyr Z may be necessary in these cases (*65*). According to our earlier suggestion (*14*), preservation of the proton during the S_1 to S_2 step in the vicinity of Mn, on base B_1 (possibly D1 Glu189), lowers the p*K* of base B (His190) which acts as the proton acceptor upon oxidation of Tyr Z. This could constitute the mechanism which ensures rapid protonation of Tyr Z$^{\bullet}$ upon its reduction, in the S_1 to S_2 step, as illustrated in Scheme 2.

(B) The S_2 to S_3 Step. In an earlier review article (*14*) we assumed that oxidation of Tyr Z in S_2 was inhibited below the temperature threshold for the S_2 to S_3 advancement and occurred concomitantly to the loss of a proton from the Mn cluster prior to its oxidation. This concerted movement relieved the constraints set by the increased positive charge in the vicinity of the Mn cluster. The subsequent finding that oxidation of Tyr Z in S_2 is possible at $T \geq 77$ K allowed for a refinement of these ideas. On the basis of the crystal structure (*66*), we suggested that His190 may form a hydrogen bond to D1 Asn298 in the S_2 state. Tyr Z and Asn298 are almost equidistant from His190, and these are the only amino acid residues found in the structure within a distance of 3 Å from the perspective nitrogen atoms of His190. Hence, formation of Tyr Z$^{\bullet}$ in S_2 is coupled to the transfer of the phenolic proton to His190, which, in its turn, relays its other proton to Asn298 (see ref *67* for an alternative view on the position of the Tyr Z−His190 couple with respect to the Mn cluster). This coupled two-proton motion is presumably inhibited at temperatures below 77 K, and this explains the temperature barrier for the formation of Tyr Z$^{\bullet}$ in S_2 (*42*). Scheme 3 depicts this model of the participation of histidine in two hydrogen bonds which facilitates the relaxation of excess positive charge. Decay of $S_2Y_Z^{\bullet}$ by charge recombination at 11 K results in the S_2^t configuration, which differs from S_2 in that unconstrained oxidation of Tyr Z in S_2^t is expected, as observed experimentally (*42*).

Scheme 3: Structural Model Showing the Possible Formation of Hydrogen Bonds between Tyr Z/His190 and His190/Asn298, Based on Crystallographic Data[a]

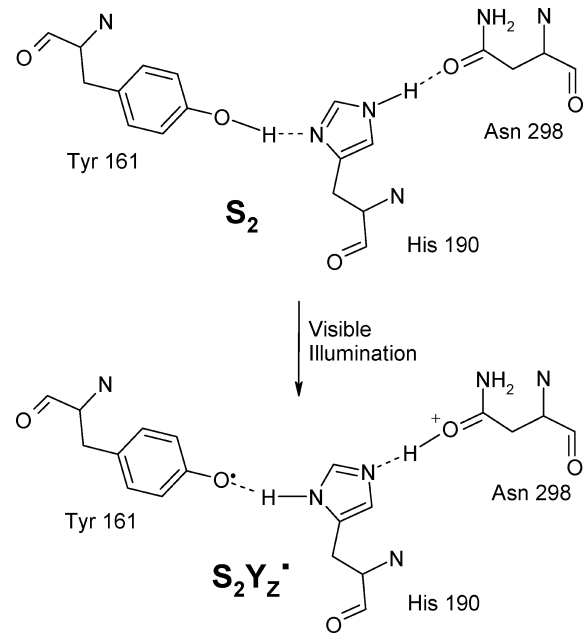

[a] See ref *66*. The His190/Asn298 hydrogen bond is proposed to exist in the S_2 state only.

In conclusion, following our previous work demonstrating the collapse of the Tyr Z•−Mn magnetic interaction above about 100 K (*47*), we present resolved spectra of Tyr Z• at X-band EPR frequency in various S states at temperatures higher than 100 K. A preliminary analysis of the $S_2Y_Z^•$ spectrum suggests a H-bonding of Tyr Z that is stronger than what has been assumed so far based on studies of Tyr D• or Tyr Z• in Mn-depleted preparations. We have also examined the temperature dependence of the recombination kinetics of the various intermediates and have observed two kinetic phases. The fastest of the two dominates at elevated temperatures and is attributed to centers where reduction of Tyr Z• is coupled to protonation (proton-coupled electron transfer, PCET). It is inferred that at ambient temperatures Tyr Z is protonated at rest. It is also proposed that $Y_Z^•/Y_ZH$ is the redox couple that oxidizes the Mn cluster during the S_1-S_2 and S_2-S_3 transitions. A simple mechanism ensuring a rapid (concerted) protonation of Tyr Z upon oxidation of the Mn cluster during the latter transitions is discussed, and also, a structure-based molecular model suggesting the participation of histidine into two hydrogen bonds, facilitating thus the relaxation of excess positive charge in S_2, is proposed.

ACKNOWLEDGMENT

We thank Dr. Y. Sanakis for help with simulations.

SUPPORTING INFORMATION AVAILABLE

Figure S1 showing spectra depicting the formation and decay of $S_2Y_Z^•$ at 150 K and Figure S2 showing the Arrhenius plot for the biphasic recombination reaction of the $S_2Y_Z^•$ radical. This material is available free of charge via the Internet at http://pubs.acs.org.

REFERENCES

1. Goussias, C., Boussac, A., and Rutherford, A. W. (2002) Photosystem II and photosynthetic oxidation of water: an overview. *Philos. Trans. R. Soc. London, Ser. B 357*, 1369–1381.
2. Diner, B. A., and Rappaport, F. (2002) Structure, dynamics, and energetics of the primary photochemistry of photosystem II of oxygenic photosynthesis. *Annu. Rev. Plant Biol. 53*, 551–580.
3. Barber, J. (2003) Photosystem II: the engine of life. *Q. Rev. Biophys. 36*, 71–89.
4. McEvoy, J. P., and Brudvig, G. W. (2006) Water-splitting chemistry of photosystem II. *Chem. Rev. 106*, 4455–4483.
5. Meyer, T. J., Huynh, M. H. V., and Thorp, H. H. (2007) The possible role of proton-coupled electron transfer (PCET) in water oxidation by photosystem II. *Angew. Chem., Int. Ed. 46*, 5284–5304.
6. McEvoy, J. P., and Brudvig, G. W. (2004) Structure-based mechanism of photosynthetic water oxidation. *Phys. Chem. Chem. Phys. 6*, 4754–4763.
7. Diner, B. A. (2001) Amino acid residues involved in the coordination and assembly of the manganese cluster of photosystem II. Proton-coupled electron transport of the redox-active tyrosines and its relationship to water oxidation. *Biochim. Biophys. Acta 1503*, 147–163.
8. Eckert, H. J., and Renger, G. (1988) Temperature dependence of P_{680}^+ reduction in O_2-evolving PSII membrane fragments at different redox states S_i of the water oxidizing system. *FEBS Lett. 236*, 425–431.
9. Rappaport, F., and Lavergne, J. (1997) Charge recombination and proton transfer in manganese-depleted photosystem II. *Biochemistry 36*, 15294–15302.
10. Junge, W., Haumann, M., Ahlbrink, R., Mulkidjanian, A., and Jurgen, C. (2002) Electrostatics and proton transferin photosynthetic water oxidation. *Philos. Trans. R. Soc. London, Ser. B 357*, 1407–1418.
11. Hoganson, C. W., and Babcock, G. T. (1997) A metalloradical mechanism for the generation of oxygen from water in photosynthesis. *Science 277*, 1953–1956.
12. Gilchrist, M. L., Ball, J. A., Randall, D. W., and Britt, R. D. (1995) Proximity of the manganese cluster of photosystem II to the redox-active tyrosine Y_Z. *Proc. Natl. Acad. Sci. U.S.A. 92*, 9545–9549.
13. Ferreira, K. N., Iverson, T. M., Maghlaoui, K., Barber, J., and Iwata, S. (2004) Architecture of the photosynthetic oxygen-evolving center. *Science 303*, 1831–1838.
14. Petrouleas, V., Koulougliotis, D., and Ioannidis, N. (2005) Trapping of metalloradical intermediates of the S-states at liquid helium temperatures. Overview of the phenomenology and mechanistic implications. *Biochemistry 44*, 6723–6728.
15. Hoganson, C. W., and Babcock, G. T. (1988) Electron-transfer events near the reaction center in O_2-evolving photosystem II preparations. *Biochemistry 27*, 5848–5855.
16. Tommos, C., Tang, X.-S., Warncke, K., Hohanson, C. W., Styring, S., McCracken, J., Diner, B. A., and Babcock, G. T. (1995) Spin-density distribution, conformation, and hydrogen bonding of the redox-active tyrosine Y_Z in photosystem II from multiple electron-magnetic resonance spectroscopies: implications for photosynthetic oxygen evolution. *J. Am. Chem. Soc. 117*, 10325–10335.
17. Tang, X.-S., Zheng, M., Chisholm, D. A., Dismukes, G. C., and Diner, B. A. (1996) Investigation of the differences in the local protein environments surrounding tyrosine radicals $Y_Z^•$ and $Y_D^•$ in photosystem II using wild-type and the D2-Tyr160Phe mutant of *Synechocystis* 6803. *Biochemistry 35*, 1475–1484.
18. Nakazawa, S., Ishii, A., Minagawa, J., and Ono, T.-a. (2005) Application of 2D-HYSCORE spectroscopy to tyrosine radicals Y_D and Y_Z in photosystem II for evaluation of spin density distributions. *Chem. Phys. Lett. 405*, 318–322.
19. Un, S., Boussac, A., and Sugiura, M. (2007) Characterization of the tyrosine-Z radical and its environment in the spin-coupled S_2Tyr Z• state of photosystem II from *Thermosynechococcus elongatus*. *Biochemistry 46*, 3138–3150.
20. Un, S., Tang, X.-S., and Diner, B. (1996) 245 GHz high-field EPR study of tyrosine-D• and tyrosine-Z• in mutants of photosystem II. *Biochemistry 35*, 679–684.
21. Boussac, A., Zimmermann, J. L., and Rutherford, A. W. (1989) EPR signals from modified charge accumulation states of the oxygen-evolving enzyme in calcium-deficient photosystem II. *Biochemistry 28*, 8984–8989.
22. MacLachlan, D. J., and Nugent, J. H. A. (1993) Investigation of the S_3 electron paramagnetic resonance signal from the oxygen-evolving complex of photosystem 2: Effect of inhibition of oxygen evolution by acetate. *Biochemistry 32*, 9772–9780.
23. Lakshmi, K. V., Eaton, S. S., Eaton, G. R., Frank, H. A., and Brudvig, G. W. (1998) Analysis of dipolar and exchange interactions between manganese and tyrosine Z in the $S_2Y_Z^•$ state of acetate-inhibited photosystem II via EPR spectral simulations at X- and Q-bands. *J. Phys. Chem. B 102*, 8327–8335.
24. Peloquin, J. M., Campbell, K. A., and Britt, R. D. (1998) ^{55}Mn pulsed ENDOR demonstrates that the photosystem II "split" EPR signal arises from a magnetically-coupled mangano-tyrosyl complex. *J. Am. Chem. Soc. 120*, 6840–6841.
25. Dorlet, P., Di Valentin, M., Babcock, G. T., and McCracken, J. L. (1998) Interaction of $Y_Z^•$ with its environment in acetate-treated photosystem II membranes and reaction center cores. *J. Phys. Chem. B 102*, 8239–8247.
26. Mino, H., and Itoh, S. (2005) The origin of split EPR signals in the Ca^{2+}-depleted photosystem II. *Photosynth. Res. 84*, 333–337.
27. Szalai, V., Kühne, H., Lakshmi, K. V., and Brudvig, G. W. (1998) Characterization of the interaction between manganese and tyrosine Z in acetate-inhibited photosystem II. *Biochemistry 37*, 13594–13603.
28. Kodera, Y., Hara, H., Astashkin, A. V., Kawamori, A., and Ono, T. (1995) EPR study of trapped tyrosine Z^+ in Ca-depleted photosystem II. *Biochim. Biophys. Acta 1232*, 43–51.
29. Feyziev, Y. M., Yoneda, D., Yoshii, T., Katsuta, N., Kawamori, A., and Watanabe, Y. (2000) Formate-induced inhibition of the water-oxidising complex of photosystem II studied by EPR. *Biochemistry 39*, 3848–3855.
30. Mino, H., Kawamori, A., and Ono, T. (2000) pH-dependent characteristics of Y_Z radical in Ca^{2+}-depleted photosystem II studied by CW-EPR and pulsed ENDOR. *Biochim. Biophys. Acta 1457*, 157–165.
31. Ioannidis, N., and Petrouleas, V. (2000) Electron paramagnetic resonance signals from the S_3 state of the oxygen-evolving complex.

A broadened radical signal induced by low-temperature near-infrared light illumination. *Biochemistry 39*, 5246–5254.
32. Geijer, P., Morvaridi, F., and Styring, S. (2001) The S_3-state of the oxygen-evolving complex in photosystem II is converted to the $S_2Y_Z^{\bullet}$ at alkaline pH. *Biochemistry 40*, 10881–10891.
33. Nugent, J. H. A., Muhiuddin, I. P., and Evans, M. C. W. (2002) Electron transfer from the water oxidizing complex at cryogenic temperatures: The S_1 to S_2 step. *Biochemistry 41*, 4117–4126.
34. Ioannidis, N., Nugent, J. H. A., and Petrouleas, V. (2002) Intermediates of the S_3 state of the oxygen-evolving complex of photosystem II. *Biochemistry 41*, 9589–9600.
35. Zhang, C., and Styring, S. (2003) Formation of split electron paramagnetic resonance signals in photosystem II suggests that tyrosineZ can be photooxidized at 5 K in the S_0 and S_1 states of the oxygen-evolving complex. *Biochemistry 42*, 8066–8076.
36. Koulougliotis, D., Shen, J. R., Ioannidis, N., and Petrouleas, V. (2003) Near-IR irradiation of the S_2 state of the water oxidizing complex of photosystem II at liquid helium temperatures produces the metalloradical intermediate attributed to $S_1Y_Z^{\bullet}$. *Biochemistry 42*, 3045–3053.
37. Nugent, J. H. A., Muhiuddin, I. P., and Evans, M. C. W. (2003) Effects of hydroxylamine on photosystem II: Reinvestigation of electron paramagnetic resonance characteristics reveals possible S state intermediates. *Biochemistry 42*, 5500–5507.
38. Zhang, C. X., Boussac, A., and Rutherford, A. W. (2004) Low-temperature electron transfer in photosystem II: A tyrosyl radical and semiquinone charge pair. *Biochemistry 43*, 13787–13795.
39. Koulougliotis, D., Teutlolf, C., Sanakis, S., Lubitz, W., and Petrouleas, V. (2004) The $S_1Y_Z^{\bullet}$ metalloradical intermediate in photosystem II: an X- and W-band EPR study. *Phys. Chem. Chem. Phys. 6*, 4859–4863.
40. Petrouleas, V., Koulougliotis, D., and Ioannidis, N. (2005) Trapping of metalloradical intermediates of the S-states at liquid helium temperatures. Overview of the phenomenology and mechanistic implications. *Biochemistry 44*, 6723–6728.
41. Su, J. H., Havelius, K. G. V., Mamedov, F., Ho, F. M., and Styring, S. (2006) Split EPR signals from photosystem II are modified by methanol, reflecting S state-dependent binding and alterations in the magnetic coupling in the $CaMn_4$ cluster. *Biochemistry 45*, 7617–7627.
42. Ioannidis, N., Zahariou, G., and Petrouleas, V. (2006) Trapping of the S_2 to S_3 state intermediate of the oxygen-evolving complex of photosystem II. *Biochemistry 45*, 6252–6259.
43. Havelius, K. G. W., Su, J. H., Feyziyev, Y., Mamedov, F, and Styring, S. (2006) Spectral resolution of the split EPR signals induced by illumination at 5 K from the S_1, S_3, and S_0 states in photosystem II. *Biochemistry 45*, 9279–9290.
44. Sioros, G., Koulougliotis, D., Karapanagos, G., and Petrouleas, V. (2007) The $S_1Y_Z^{\bullet}$ metalloradical EPR signal of photosystem II contains two distinct components that advance respectively to the multiline and $g = 4.1$ conformations of S_2. *Biochemistry 46*, 210–217.
45. Boussac, A., Sugiura, M., Lai, T.-L., and Rutherford, A. W. (2008) Low temperature photochemistry in photosystem II from *Thermosynechococcus elongatus* induced by visible and near-infrared light. *Philos. Trans. R. Soc. London, Ser. B 363*, 1203–1210.
46. Su, J.-H., Havelius, K. G. V., Ho, F. M., Han, G., Mamedov, F., and Styring, S. (2007) Formation spectra of the EPR split signals from the S0, S1, and S3 states in photosystem II induced by monochromatic light at 5 K. *Biochemistry 46*, 10703–10712.
47. Zahariou, G., Ioannidis, N., Sioros, G., and Petrouleas, V. (2007) The collapse of the tyrosine $Z^{\bullet}$-Mn spin-spin interaction above approximately 100 K reveals the spectrum of tyrosine $Z^{\bullet}$. An application of rapid-scan EPR to the study of intermediates of the water splitting mechanism of photosystem II. *Biochemistry 46*, 14335–14341.
48. Fielding, L., More, K. M., Eaton, G. R., and Eaton, S. S. (1986) Metal-nitroxyl interactions. 51. Collapse of iron-nitroxyl electron-electron spin-spin splitting due to the increase in the electron spin relaxation rate for high-spin iron(III) when temperature is increased. *J. Am. Chem. Soc. 108*, 8194–8196.
49. Ford, R. C., and Evans, M. C. W. (1983) Isolation of a photosystem-2 preparation from higher-plants with highly enriched oxygen evolution activity. *FEBS Lett. 160*, 159–164.
50. Ioannidis, N., Schansker, G., Barynin, V. V., and Petrouleas, V. (2000) Interaction of nitric oxide with the oxygen evolving complex of photosystem II and manganese catalase: a comparative study. *J. Biol. Inorg. Chem. 5*, 354–363.
51. Svistunenko, D. A., and Cooper, C. E. (2004) A new method of identifying the site of tyrosyl radicals in proteins. *Biophys. J. 87*, 582–595.
52. Hofbauer, W., Zouni, A., Bittl, R., Kern, J., Orth, P., Lendzian, F., Fromme, P., Witt, H. T., and Lubitz, W. (2001) Photosystem II single crystals studied by EPR spectroscopy at 94 GHz: The tyrosine radical $Y_D^{\bullet}$. *Proc. Natl. Acad. Sci. U.S.A. 98*, 6623–6628.
53. Ivancich, A., Mattioli, A. T., and Un, S. (1999) Effect of protein microenvironment on tyrosyl radicals. A high-field (285 GHz) EPR, resonance Raman, and hybrid density functional study. *J. Am. Chem. Soc. 121*, 5743–5753.
54. Fasanella, E. L., and Gordy, W. (1969) Electron spin resonance of an irradiated single crystal of L-tyrosine-HCl. *Proc. Natl. Acad. Sci. U.S.A. 62*, 299–304.
55. Frey, M. N., Koetzle, T. F., Lehmann, M. S., and Hamilton, W. C. (1973) Precision neutron diffraction structure determination of protein and nucleic acid components. X. A comparison between the crystal and molecular structures of L-tyrosine and L-tyrosine hydrochloride. *J. Chem. Phys. 58*, 2547–2556.
56. Rappaport, F., Guergova-Kuras, M., Nixon, P. J., Diner, B. A., and Lavergne, J. (2002) Kinetics and pathways of charge recombination in photosystem II. *Biochemistry 41*, 8518–8527.
57. Grabolle, M., and Dau, H. (2005) Energetics of primary and secondary electron transfer in photosystem II membrane particles of spinach revisited on basis of recombination-fluorescence measurements. *Biochim. Biophys. Acta 1708*, 209–218.
58. Tommos, C., and Babcock, G., T. (2000) Proton and hydrogen currents in photosynthetic water oxidation. *Biochim. Biophys. Acta 1458*, 199–219.
59. Pieper, J., Hauss, T., Buchsteiner, A., Baczyñski, K., Adamiak, K., Lechner, R. E., and Renger, G. (2007) Temperature- and hydration-dependant protein dynamics in photosystem II of green plants studied by quasielastic neutron scattering. *Biochemistry 46*, 11398–11409.
60. Renger, G. (2004) Coupling of electron and proton transfer in oxidative water cleavage in photosynthesis. *Biochim. Biophys. Acta 1655*, 195–204.
61. Debus, R. J., Campbell, K. A., Pham, D. P., Hays, A.-M. A., and Britt, R. D. (2000) Glutamate 189 of the D1 polypeptide modulates the magnetic and redox properties of the manganese cluster and tyrosine Y_Z in photosystem II. *Biochemistry 39*, 6275–6287.
62. Nugent, J. H. A., Rich, A. M., and Evans, M. C. W. (2001) Photosynthetic water oxidation: towards a mechanism. *Biochim. Biophys. Acta 1503*, 138–146.
63. Diner, B. A. (2005) The redox-active tyrosines Y_Z and Y_D, in *Photosystem II: The Light-Driven Water:Plastoquinone Oxidoreductase* (Wydrzynski, T., and Satoh, K., Eds.) pp 207−233, Springer, Amsterdam, The Netherlands.
64. Vass, I., and Styring, S. (1991) pH-dependent charge equilibria between tyrosine-D and the S states in photosystem II. Estimation of relative midpoint redox potentials. *Biochemistry 30*, 830–839.
65. Szalai, V. A., and Brudvig, G. W. (1996) Reversible binding of nitric oxide to tyrosyl radicals in photosystem II. Nitric oxide quenches formation of the S3 EPR signal species in acetate-inhibited photosystem II. *Biochemistry 35*, 15080–15087.
66. Loll, B., Kern, J., Saenger, W., Zouni, A., and Biesiadka, J. (2005) Towards complete cofactor arrangement in the 3.0 Å resolution structure of photosystem II. *Nature 438*, 1040–1044.
67. Zhang, C. (2007) Low-barrier hydrogen bond plays key role in active photosystem II—A new model for photosynthetic water oxidation. *Biochim. Biophys. Acta 1767*, 493–499.

BI800390R